Constrained Optimization-Based Yaw-Rate Reference Map Generation for Active Rear Steering Control of Four-Wheel-Steering Vehicles

Myeongseok Ryu[1], Donghyun Hwang[2], Youngsik Yoon[3], and Kyunghwan Choi[4*]

[1]Cho Chun Shik Graduate School of Mobility, Korea Advanced Institute of Science and Technology (KAIST), Daejeon, 34051, Korea (dding_98@kaist.ac.kr)
[2]Vehicle Motion Control Development Team, Hyundai Motor Company (HMC), Hwaseong, 18280, Korea (hdh0914@hyundai.com)
[3]Vehicle Motion Control Development Team, Hyundai Motor Company (HMC), Hwaseong, 18280, Korea (ys_yoon@hyundai.com)
[4]Cho Chun Shik Graduate School of Mobility, Korea Advanced Institute of Science and Technology (KAIST), Daejeon, 34051, Korea (kh.choi@kaist.ac.kr) * Corresponding author

Abstract: The effectiveness of active rear steering (ARS) for four-wheel-steering (4WS) vehicles is widely recognized in the automotive industry. At low speeds, ARS can enhance maneuverability by steering the rear wheels in the opposite direction to the front wheels, reducing the turning radius. In contrast, at high speeds, ARS can improve stability by steering the rear wheels in the same direction as the front wheels, preventing oversteer behavior. However, the performance of ARS is often limited by the reference model used to generate the desired yaw rate, which is typically derived from a steady-state of front-wheel-steering (FWS) vehicle model. In this paper, we conduct a numerical analysis to construct an optimal reference map for ARS control by formulating an constrained optimization problem. In the optimization problem, safety constraints are imposed to ensure that the vehicle operates within safe limits. Numerical simulations demonstrates the effectiveness of the proposed method in providing an optimal reference map for ARS control.

Keywords: Active Rear Steering (ARS), Four-Wheel Steering (4WS), Vehicle Dynamics, Constrained Optimization

1 INTRODUCTION

The active rear steering (ARS) improves the conventional front-wheel-steering (FWS) system by adding the capability to steer the rear wheels, thereby enhancing vehicle maneuverability and stability. The control strategies for ARS had been widely studied in past decades in 1980s and 1990s. However, the commercialization was limited due to the cost and complexity of the system [1]. In recent, owing to advance of electronic control technology, the ARS has gained renewed attention, and several modern control strategies have been proposed in the literature [2–12].

Across the various control strategies, the core concept of ARS control is to generate larger yaw rate at low speeds by steering the rear wheels in the opposite direction to the front wheels, and to reduce sideslip angle at high speeds by steering the rear wheels in the same direction as the front wheels [2]. These control behaviors result in improved maneuverability and enhanced stability at slow and high speeds, respectively, which are the key performance metrics for vehicle control.

Related works are reviewed including ARS and 4WS control methods. Motivated by the above concept, conventionally, literature has adopted velocity-dependent ratios of rear steering angle to front steering angle, which typically called proportional control [2, 3]. In [4], phase delay and phase reversal control methods were proposed, which mitigate the phase difference between yaw rate and lateral acceleration, and improve the transient response of the vehicle, respectively. In addition, owing to the fact that steering angle is limited at high speeds, steering-angle-dependent ratio was proposed in [5]. Regardless of vehicle velocity, the rear steering angle is steered in the same0 (opposite) direction to the front steering angle when the front steering angle is small (large).

Over the feedforward control, feedback control strategies also have been proposed. Representatively, yaw rate tracking control methods have been adopted, which control the rear steering angle to track a reference yaw rate, using various control techniques, such as proportional-integral-derivative (PID) control [6], sliding mode control (SMC) [7–9], H-infinity control [10], and neuro-adaptive control (NAC) [12]. Furthermore, zero-dynamics-based control methods have been proposed, which assume that sideslip angle is zero. However, as reported in [6, 11], the sideslip angle is non-minimum phase, if the yaw rate is used as the only output of the system, when tire characteristics are saturated. To address this issue, [6] proposed a control methods that considers both yaw rate and sideslip angle in a weighted sum, and stable range of the weighting factor is proposed to ensure the stability of the system.

However, although the effectiveness of ARS control has been widely recognized and demonstrated, the performance of ARS control is often limited by the reference model used to generate the desired yaw rate, which is typically derived from front-wheel-steering (FWS) vehicle model at steady state [9, 11]. Hence, the fact that ARS can improve yaw rate (maneuverability) while remaining the sideslip angle (stability) within safe limits is not fully exploited, which motivates the need for an optimal reference map for ARS control. Thus, in this paper, we conduct a numerical analysis to construct an optimal refer-

Table 1. Vehicle Parameters.

Symbol	Description	Value
m	Mass	2335.07 kg
h	Height of CG	0.42 m
w	Track width	1.627 m
ρ	Roll ratio	0.6
I_z	Yaw moment of inertia	5376.432 kg m^2
l_f	Distance from CG to front axle	1.574 m
l_r	Distance from CG to rear axle	1.566 m
C_f	Cornering stiffness of front tires	119.54 kN rad^{-1}
C_r	Cornering stiffness of rear tires	119.83 kN rad^{-1}

ence map for ARS control by formulating a constrained optimization problem.

This paper is organized as follows. In Section 2, the vehicle model used in the numerical analysis is introduced. In Section 3, the constrained optimization problem for constructing the optimal reference map for ARS control is formulated, and the optimization results are analyzed. In Section 4, the optimization results are employed as a reference map for ARS control, and numerical simulations are conducted to validate the effectiveness of the proposed approach in improving the performance of ARS control for 4WS vehicles. Finally, in Section 5, the paper is concluded with a summary of the findings and future work.

2 VEHICLE MODELLING

In this section, we introduce the vehicle model used for the numerical analysis. The parameters of the vehicle model are listed in Table 1.

We adopt a 2-DOF bicycle model presented in [13, Sec. 2.6], as follows:

$$\frac{\mathrm{d}}{\mathrm{d}t}\begin{pmatrix}\beta\\ r\end{pmatrix} = \begin{pmatrix}\frac{1}{mv_x}(F_{y,f}+F_{y,r})-r\\ \frac{1}{I_z}(l_fF_{y,f}-l_rF_{y,r})\end{pmatrix}, \tag{1}$$

where β and r are the sideslip angle and yaw rate of the vehicle, respectively; v_x is the longitudinal velocity of the vehicle; and $F_{y,i}$ is the lateral tire force at front ($i=f$) and rear ($i=r$) tires, respectively.

The lateral tire forces are represented as nonlinear functions of the slip angles α_i and the normal forces $F_{z,i}$ for all $i \in \{f,r\}$. We adopt the magic formula for the lateral tire forces in [13, Sec. 13.5], as follows:

$$\begin{aligned}F_{y,i} =& D_{y,i}\sin\left[C_{y,i}\tan^{-1}\left\{B_{y,i}\alpha_{y,i}-E_{y,i}\right.\right.\\ &\left.\left.\left(B_{y,i}\alpha_{y,i}-\tan^{-1}(B_{y,i}\alpha_{y,i})\right)\right\}\right]+S_{y,i},\end{aligned} \tag{2}$$

where $\alpha_{y,i} = \alpha_{i,y} + S_{y,i}$. The coefficients $B_{y,i}$, $C_{y,i}$, $D_{y,i}$, and $E_{y,i}$ are the stiffness, shape, peak, and curvature factors, and $S_{y,Hy}$ and $S_{y,Vy}$ are the horizontal and vertical shifts, and γ is the camber angle. These coefficients are obtained from 245/46R19 and 275/40R19 tire models for the front and rear tires, respectively, under air pressure of 241 kPa. The tire forces are illustrated in

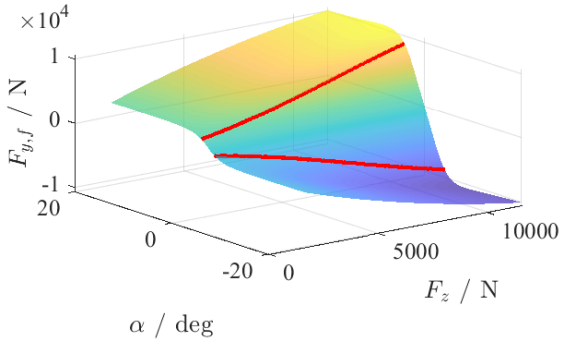

(a) Front tire forces (245/46R19 at 241 kPa).

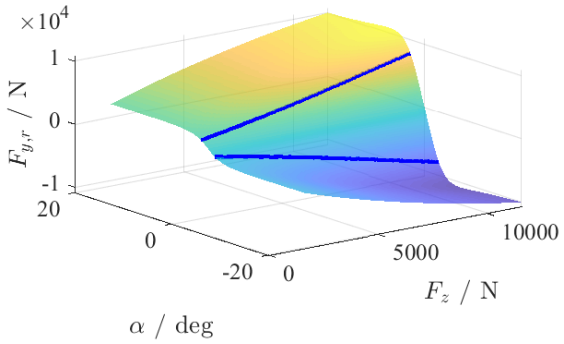

(b) Rear tire forces (275/40R19 at 241 kPa).

Fig. 1. Lateral tire forces as functions of slip angles and normal forces. Red solid line [—] and blue solid line [—] indicate bounds of the linear region of the tire forces for the front and rear tires, respectively.

Fig. 1, with respect to slip angles and normal forces. In addition, the slip angles are defined as follows:

$$\alpha_f = \beta + \tfrac{l_f}{v_x}r - \delta_f, \quad \alpha_r = \beta - \tfrac{l_r}{v_x}r - \delta_r, \tag{3}$$

assuming small angles for β, r, δ_f, and δ_r.

3 NUMERICAL ANALYSIS

3.1 Optimization Problem Formulation

In this section, a constrained optimization problem for constructing the optimal reference map for ARS control is formulated. The vehicle parameters and dynamics used in the optimization problem are introduced in Section 2. The optimization problem is formulated as follows:

$$\min_{\delta_r} \quad J(\delta_f) = -r^2 + \lambda\beta^2 \tag{4a}$$

$$\text{subject to} \quad \tfrac{\mathrm{d}}{\mathrm{d}t}\beta = \tfrac{\mathrm{d}}{\mathrm{d}t}r = 0, \tag{4b}$$

$$|\beta| \le \overline{\beta}, \tag{4c}$$

$$|a_{y,i}| \le \overline{a}_{y,i}, \ \forall i \in \{f,r\} \tag{4d}$$

$$|\alpha_i| \le \overline{\alpha}_i, \ \forall i \in \{f,r\} \tag{4e}$$

$$|\delta_r| \le \overline{\delta}_r, \tag{4f}$$

where $J := J(\delta_r)$ is the objective function, $\lambda \in \mathbb{R}_{>0}$ denotes the weighting factor, and $\overline{\beta}, \overline{a}_{y,i}, \overline{\alpha}_i, \overline{\delta}_r \in \mathbb{R}_{>0}$

Table 2. Comparison of Optimization Configurations.

	Optimization Configuration
FWS	Front wheel steering only ($\delta_r = 0$, $\lambda = 100$)
ARS-1	Low penalty on sideslip angle ($\lambda = 100$)
ARS-2	High penalty on sideslip angle ($\lambda = 3000$)

are the magnitude bounds for the sideslip angle, lateral acceleration, slip angle, and rear steering angle, respectively, for all $i \in \{f, r\}$.

The objective function (4a) is designed to maximize the yaw rate and minimize the sideslip angle, which is a common performance metric for vehicle maneuverability and stability. By tuning the weighting factor λ, the priority between maneuverability and stability can be adjusted, which is crucial for lateral vehicle control. The analysis is conducted under the steady-state condition, which is represented by the first constraint (4b). The remaining constraints (4c)–(4f) are safety constraints that ensure the vehicle operates within safe limits at the steady-state condition, with $\overline{\beta} = 3°$, $\overline{a}_{y,i} = 0.8\,\mathrm{g}$, and $\overline{\delta_r} = 3.5°$.

Although the Magic Formula (2) provides a more accurate description of nonlinear lateral tire forces, directly embedding it into the optimization problem (4) may lead to a highly nonlinear and potentially ill-conditioned optimization problem. Therefore, to ensure a well-posed and numerically tractable formulation, the vehicle dynamics are described using a linear tire model within the locally valid tire region, i.e., $F_{y,i} = C_i \alpha_i$, where $C_i = D_{y,i}$ is the cornering stiffness of the tire for all $i \in \{f, r\}$. The nonlinear tire characteristics are instead incorporated through slip-angle constraints, whose admissible bounds are determined from the Magic Formula in (4e), which is illustrated in Fig. 1 as red solid line and blue solid line for the front and rear tires, respectively, i.e., 10% deviation from the linear region is allowed.

Moreover, considering lateral acceleration, the normal forces are calculated using static weight distribution [14, Sec. 18.3], as follows:

$$\begin{pmatrix} F_{z,fl} \\ F_{z,fr} \\ F_{z,rl} \\ F_{z,rr} \end{pmatrix} = \begin{pmatrix} \frac{mgl_r}{2(l_f+l_r)} \\ \frac{mgl_f}{2(l_f+l_r)} \\ \frac{mgl_r}{2(l_f+l_r)} \\ \frac{mgl_r}{2(l_f+l_r)} \end{pmatrix} + \begin{pmatrix} -\rho\frac{ma_y h}{2w} \\ +\rho\frac{ma_y h}{2w} \\ -(1-\rho)\frac{ma_y h}{2w} \\ +(1-\rho)\frac{ma_y h}{2w} \end{pmatrix}, \quad (5)$$

where subscripts fl, fr, rl, and rr denote the front-left, front-right, rear-left, and rear-right tires, respectively; and $g = 9.81$ is the gravitational acceleration.

3.2 Analysis Results

The optimization problem (4) is solved for various longitudinal velocities $v_x \in \{20, \cdots, 110\}\ \mathrm{km\,h^{-1}}$, and front wheel angles $\delta_f \in \{0.1, \cdots, 10\}\ °$. Three configurations are compared, as listed in Table 2. The optimization results are illustrated in Figs. 2. Furthermore, the optimization result at $\delta_f = 4.0°$, is highlighted in Fig. 3 with quantitative comparison in Table 3.

In Fig. 2a, the optimization results for the FWS configuration, show that the operating domain, v_x and δ_f, is limited due to the safety constraints, and the maximum yaw rates are low compared to the ARS configurations. Moreover, since the rear wheels are not steered, the sideslip angles are passively determined by the front wheel steering.

In contrast, in Figs. 2b and 2c, the optimization results for the ARS configurations show that the operating domain is significantly expanded, and the maximum yaw rates are improved, as well. This demonstrates the effectiveness of ARS control in enhancing the maneuverability of 4WS vehicles, ensuring the vehicle operates within safe limits. Specifically, at 40–45 $\mathrm{km\,h^{-1}}$, the maximum yaw rates are significantly improved when the front wheel angle is $4.0°$.

The effect of the weighting factor λ in the objective function is also observed in Figs. 2b and 2c. By increasing the weighting factor λ, the maximum yaw rates are reduced, but the sideslip angles are around zero in wide operating domain, by starting steering the rear wheels in the same direction at lower speeds. It is notable that red solid line in Figs. 2b and 2c indicates the phase conversion, which implies that higher weighting factor λ leads to earlier phase conversion with respect to longitudinal velocity.

Additionally, the ideal rear steering strategies at steady state for the ARS configurations can be observed in Figs. 2b and 2c. As shown in Figs. 2b and 2c, the optimal rear steering angles δ_r are negative at low speeds, which indicates that the rear wheels are steered in the opposite direction to the front wheels, while the optimal rear steering angles δ_r are positive at high speeds, which indicates that the rear wheels are steered in the same direction as the front wheels.

We detail comparison of the optimization results, especially at $\delta_f = 4.0°$, in Fig. 3. As shown in Fig. 3, the yaw rates of the ARS configurations are significantly improved compared to the FWS configuration, while the sideslip angles are maintained within the safety limits. Quantitatively, as shown in Table 3, the maximum yaw rate is improved by 74.7% and 38.1% for ARS-1 and ARS-2 configurations, respectively, compared to the FWS configuration, while the minimum absolute value of the sideslip angle is reduced by 1.9% and 97.3%, respectively, at $v_x = 43.9\,\mathrm{km\,h^{-1}}$. Moreover, according to increasing the weighting factor λ from ARS-1 to ARS-2, the maximum yaw rates are reduced, but the sideslip angles are significantly reduced; specifically, the sideslip angles are almost 0 when $22.5 \leq v_x \leq 55\ \mathrm{km\,h^{-1}}$.

4 NUMERICAL VALIDATION

4.1 Validation Setup

In this section, the optimization results are employed as a reference map for ARS control, and numerical simulations are conducted to validate the effectiveness of the

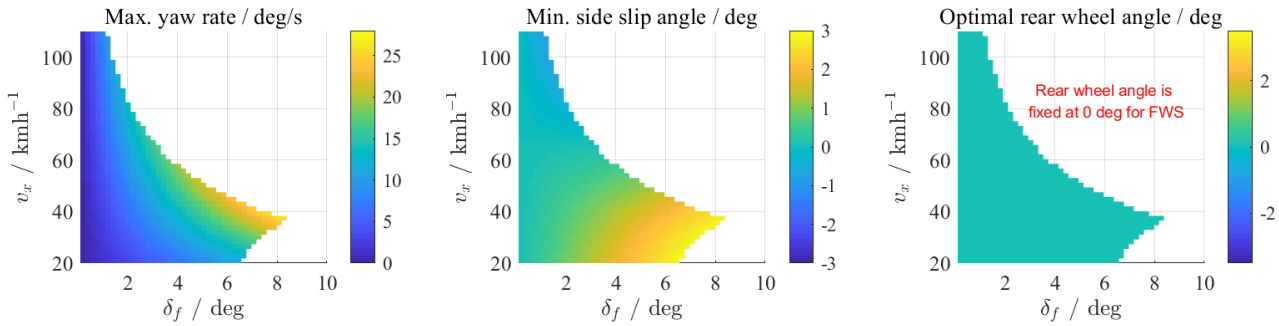

(a) FWS configuration.

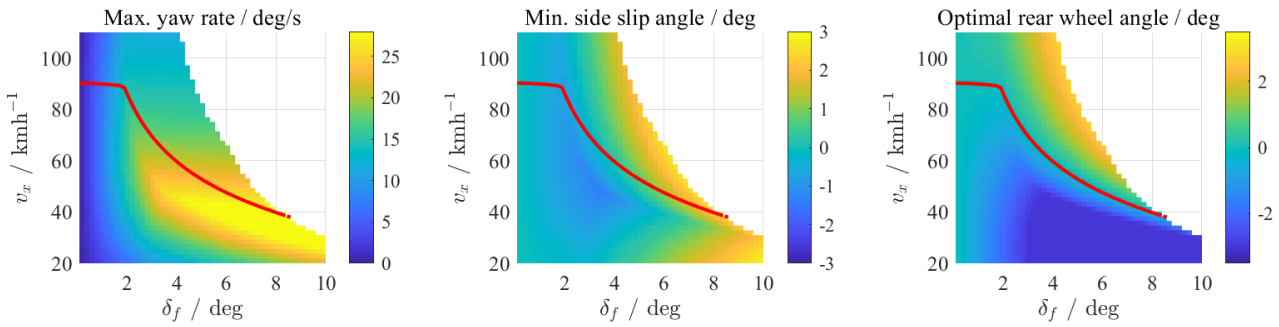

(b) ARS-1 configuration (low beta penalty).

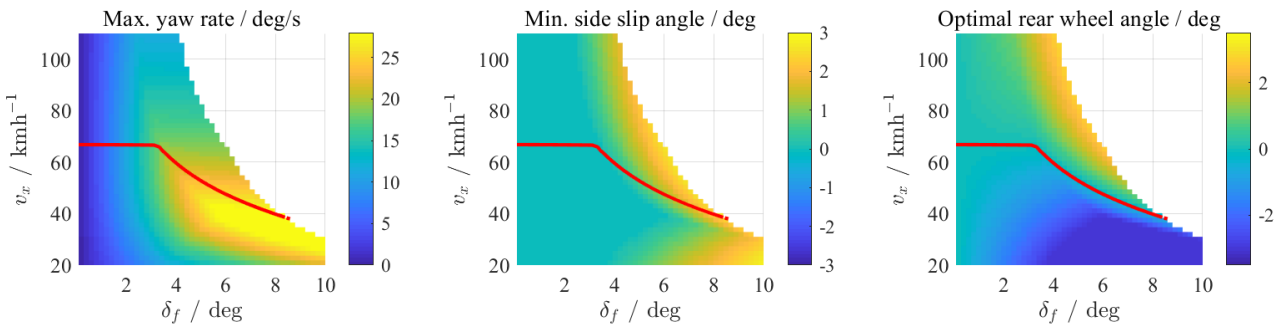

(c) ARS-2 configuration (high beta penalty).

Fig. 2. Optimization results of (4) for various longitudinal velocities v_x and front steering angles δ_f. Red solid line [—] indicates phase conversion from opposite-phase rear steering at low speeds to same-phase rear steering at high speeds.

Table 3. Optimization Results at $\delta_f = 4.0°$, and $v_x = 43.9\,\mathrm{km\,h^{-1}}$.

	Max. Yaw Rate r	**Min. Sideslip Angle** $\lvert\beta\rvert$
FWS	15.35 °/s (-)	1.101° (-)
ARS-1	26.82 °/s (+74.7%)	1.08° (-1.9%)
ARS-2	21.35 °/s (+38.1%)	0.03° (-97.3%)

proposed approach in improving the performance of ARS control for 4WS vehicles.

The vehicle parameters used in the simulations are the same as those used in the optimization problem. Test scenarios are designed as step steering inputs at $v_x = 42.5\,\mathrm{km\,h^{-1}}$. The driver's command is a step steering input from 0° to 90° at $t = 10\,\mathrm{s}$, under 300 °/s rate limit of the steering wheel. The steering wheel angle of 90° corresponds to the front wheel angle δ_f of 6.75°.

The yaw rate tracking controller for ARS is designed as a simple proportional-integral (PI) controller, as follows:

$$\delta_r(t) = K_p(r_{\mathrm{ref}}(t) - r(t)) + K_i \int_0^t (r_{\mathrm{ref}}(\tau) - r(\tau))\mathrm{d}\tau, \tag{6}$$

where $r_{\mathrm{ref}}(t)$ is the reference yaw rate obtained from the optimization results, and $K_p = 0.01$ and $K_i = 1$ are the proportional and integral gains, respectively. The reference yaw rate is obtained by linearly interpolating the maximum yaw rate of the optimization results for the given longitudinal velocity and front steering angle.

The simulation is implemented in IPG CarMaker [15], which is a widely used vehicle dynamics simulation software in the automotive industry. The sampling time is set to 1 ms for simulation, and 10 ms for the controller.

For comparative study, the reference map obtained from ARS-2 configuration is employed for ARS control (denoted as (C_1)), and the reference map obtained from FWS configuration is employed for FWS control (de-

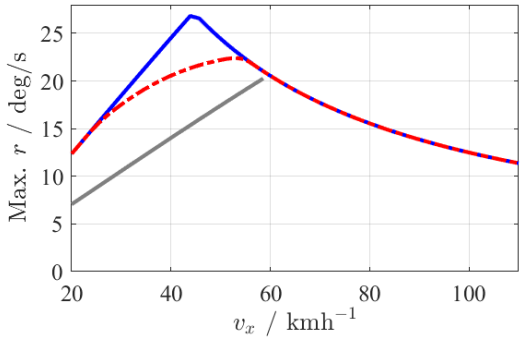

(a) Yaw rates r.

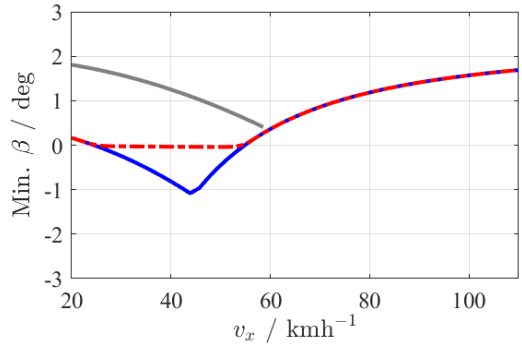

(b) Sideslip angles β.

Fig. 3. Yaw rates and sideslip angles at $\delta_f = 4.0°$ of FWS [—] and ARS-1 [—], and ARS-2 [- - -].

noted as (C_2)).

4.2 Validation Results

The simulation result is illustrated in Fig. 4 and quantitatively compared in Table 4.

As shown in Fig. 4, (C_1) utilized the capability of ARS control to generate larger yaw rate while maintaining the sideslip angle within the safety limits, i.e., $|\beta| \leq 3°$. In contrast, the yaw rate of (C_2) is lower than that of (C_1) around 9.2% at the steady state, as shown in Table 4. This is because the target yaw rate of (C_2) is generated assuming the ARS control is unavailable, resulting in a lower target yaw rate compared to (C_1).

It should be noted that the sideslip angle of (C_1) is higher than that of (C_2). This implies the effect of ARS in opposite-directional rear steering. Increasing the magnitude of opposite-directional rear steering, the sideslip angle is biased toward negative direction. Considering this effect, the weighting factor λ in the optimization problem (4) should be carefully tuned. Smaller weighing factor λ in the optimization problem may lead to higher optimal reference yaw rate, but it may also lead to higher sideslip angle, which can affect the stability of the vehicle. On the other hand, higher weighing factor λ may lead to more safe reference yaw rate, but it may affect the maneuverability of the vehicle by reducing the reference yaw rate.

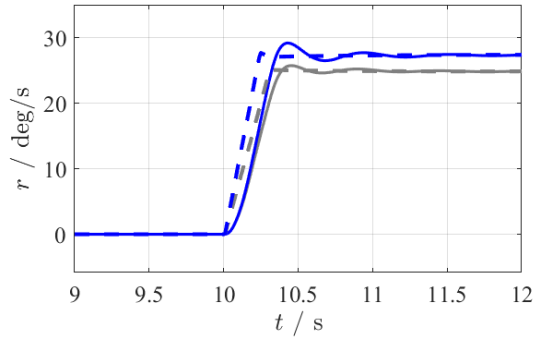

(a) Yaw rates r.

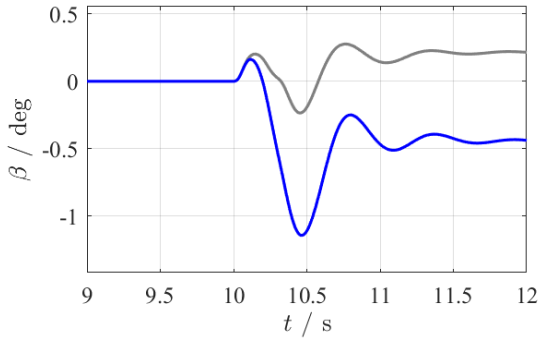

(b) Sideslip angles β.

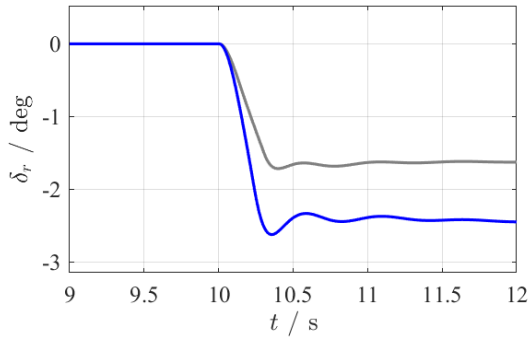

(c) Rear steering angles δ_r.

Fig. 4. Simulation results of (C_1) [—] and (C_2) [—] at $v_x = 42.5\,\mathrm{km\,h^{-1}}$ and 90° step steering scenarios. Yaw rate references are illustrated as [- - -] and [- - -] for (C_1) and (C_2), respectively.

5 CONCLUSION

In this paper, we analyzed the effectiveness of active rear steering (ARS) control for four wheel steering (4WS) vehicles by formulating a constrained optimization problem to construct an optimal reference yaw rate map. The optimization problem was designed to maximize the yaw rate of the vehicle while minimizing the sideslip angle, subject to safety constraints that ensure the vehicle operates within safe domains. The optimization results demonstrated that ARS control can significantly expand the feasible operating regions and improve the maximum yaw rates.

Table 4. Quantitative Comparison of Simulation Results.

	Max. Yaw Rate r	**Min. Sideslip Angle** $\lvert\beta\rvert$
(C_1) [ ]	$27.39\,°/s$	$0.44°$
(C_2) [ ]	$24.86\,°/s$	$0.22°$

Moreover, the optimization results were employed as a reference yaw rate map for ARS control, and numerical simulations were conducted to validate the effectiveness of the proposed approach in improving yaw rate while maintaining the sideslip angle within safety limits.

As future work, the reference map will be employed in advanced ARS control strategies, such as model predictive control (MPC) and real-time implementation on Electronic Control Units (ECUs) for real-world testing and validation.

ACKNOWLEDGEMENT

This work was supported in part by Hyundai Motor Company (HMC).

REFERENCES

[1] H.-S. Park and M.-S. Kim, "Development of a path tracker based on a 4ws vehicle for low-speed automated driving systems," *Applied Sciences*, vol. 15, no. 6, 2025. [Online]. Available: https://www.mdpi.com/2076-3417/15/6/3043

[2] Y. H. Cho and J. Kim, "Design of optimal four-wheel steering system," *Vehicle System Dynamics*, vol. 24, no. 9, pp. 661–682, 1995. [Online]. Available: https://doi.org/10.1080/00423119508969112

[3] L. Bredthauer and D. Lynch, "Use of active rear steering to achieve desired vehicle transient lateral dynamics," in *SAE Technical Paper Series*, no. 2018-01-0565. 400 Commonwealth Drive, Warrendale, PA, United States: SAE International, Apr. 2018. [Online]. Available: https://doi.org/10.4271/2018-01-0565

[4] T. Eguchi, Y. Sakita, K. Kawagoe, S. Kaneko, K. Mori, and T. Matsumoto, "Development of "super hicas", a new rear wheel steering system with phasereversal control," *SAE Transactions*, vol. 98, pp. 1495–1504, 1989. [Online]. Available: http://www.jstor.org/stable/44472394

[5] S. Sano, Y. Furukawa, and S. Shiraishi, "Four wheel steering system with rear wheel steer angle controlled as a function of sterring wheel angle," *SAE Transactions*, vol. 95, pp. 880–893, 1986. [Online]. Available: http://www.jstor.org/stable/44725442

[6] Y. Guan, H. Zhou, Z. He, and H. Liu, "Enhancing yaw tracking stability in 4ws vehicles: An output redefinition approach to overcoming nonminimum-phase challenges," in *2024 39th Youth Academic Annual Conference of Chinese Association of Automation (YAC)*, 2024, pp. 1211–1216.

[7] P. I. Ro and H. Kim, "Four wheel steering system for vehicle handling improvement: A robust model reference control using the sliding mode," *Proceedings of the Institution of Mechanical Engineers, Part D: Journal of Automobile Engineering*, vol. 210, no. 4, pp. 335–346, 1996. [Online]. Available: https://doi.org/10.1243/PIME_PROC_1996_210_280_02

[8] M. Akar, "Yaw rate and sideslip tracking for 4-wheel steering cars using sliding mode control," in *2006 IEEE Conference on Computer Aided Control System Design, 2006 IEEE International Conference on Control Applications, 2006 IEEE International Symposium on Intelligent Control*, 2006, pp. 1300–1305. [Online]. Available: https://doi.org/10.1109/CACSD-CCA-ISIC.2006.4776830

[9] T. Khanke, S. Chaudhari, S. Phadke, and P. Shendge, "Yaw stability of 4ws with variable steering ratio strategy using inertial delay control based sliding mode control," in *2019 International Conference on Communication and Electronics Systems (ICCES)*, 2019, pp. 521–526.

[10] H.-M. Lv, N. Chen, and P. Li, "Multi-objective h ∞ optimal control for four-wheel steering vehicle based on yaw rate tracking," *Proceedings of the Institution of Mechanical Engineers, Part D*, vol. 218, no. 10, pp. 1117–1123, 2004. [Online]. Available: https://doi.org/10.1177/095440700421801006

[11] X. Hu, P. Wang, S. Cai, L. Zhang, Y. Hu, and H. Chen, "Vehicle stability analysis by zero dynamics to improve control performance," *IEEE Transactions on Control Systems Technology*, vol. 31, no. 6, pp. 2365–2379, 2023.

[12] M. Ryu and K. Choi, "All-wheel steering vehicle control based on contraction theory with neural network," in *2026 IEEE 19th International Conference on Advanced Motion Control (AMC)*, 2026, pp. 1–6.

[13] R. Rajamani, *Vehicle Dynamics and Control*, ser. Mechanical Engineering Series. Springer US, 2011. [Online]. Available: https://books.google.co.kr/books?id=cZJFDox4KuUC

[14] W. F. Milliken and D. L. Milliken, *Race Car Vehicle Dynamics*. Great Britain: Society of Automotive Engineers Inc., 1996.

[15] IPG Automotive, "CarMaker: The simulation solution for virtual test driving," https://www.ipg-automotive.com/solutions/product-portfolio/carmaker, 2026, accessed: 2026-05-29.